Eur. Phys. J. B **34**, 237–246 (2003)
DOI: 10.1140/epjb/e2003-00217-1

THE EUROPEAN PHYSICAL JOURNAL B

Magnetoconductance oscillations in semiconductor–superconductor junctions with a laterally isolating barrier layer inside semiconductor region

Young-Chung Hsue[1], Tzong-Jer Yang[1], Ben-Yuan Gu[2,a], and Jian Wang[3]

[1] Department of Electrophysics, National Chiao Tung University, Hsinchu, 30050, Taiwan
[2] Institute of Physics, The Chinese Academy of Sciences, PO Box 603, Beijing 100080, PR China
[3] Department of Physics, The University of Hong Kong, Pokfulam Road, Hong Kong, PR China

Received 29 May 2002 / Received in final form 21 March 2003
Published online 4 August 2003 –

Abstract. The oscillatory characteristics of magnetoconductance for a junction composed of a superconductor and a semiconductor, in which two parallel quantum wave guides are coupled with each other through a potential barrier layer, are studied systematically. To model the imperfectness of the interface, we introduce a $\delta-$function scattering potential barrier lying close to the interface of the junction. The magnetoconductance oscillations (MCO) in this system stem from two sources: one is the interference of wave functions of quasi-particles due to multiple Andreev reflections at the interface; the other is attributed to the variation of the number of the propagation modes when introducing the isolating barrier layer. The introduction of the isolating layer in the quantum wave-guides strongly modifies MCO. We also present a physical picture for the MCO based on a phenomenological argument. The theoretically fitted results are in good agreement with numerical ones.

PACS. 73.40.-c Electronic transport in interface structures – 74.80.Fp Point contact; SN and SNS junctions – 73.21.Hb Quantum wires – 85.35.Be Quantum well devices (quantum dots, quantum wires, etc.)

1 Introduction

In recent years the transport properties of quasiparticles (QPs) in normal-conductor-superconductor "hybrid" mesoscopic structures have attracted much attention [1–4]. Many interesting phenomena have been revealed in various "hybrid" mesoscopic systems, for instance, normal-metal-superconductor (NS) junctions, or $S-I-S$, $S-N-S$, $S-I-N$, $N-I-N-S$ junctions [5–14]. Many of the novel characteristics of the NS junctions originate from the well-known Andreev reflection (AR) [13]: An electron excitation above the Fermi level in the normal metal is reflected at the normal-metal-superconductor (NS) interface as a hole excitation below the Fermi level. The missing charge of $2e$ is converted to a supercurrent.

Most of the present technological efforts in this area are aimed at fabricating a direct contact between a superconducting film and the two-dimensional electron gas (2DEG) in a semiconductor heterostructure. The transport of the QPs can be made ballistically by employing a high-mobility 2DEG confined in a semiconductor heterostructure. Such a "hybrid" system would be affected by both AR and mesoscopic effects. Recently, superconductor–semiconductor–superconductor (S–Sm–S) junctions have been realized in strong magnetic fields [15,16].

The origin of the magnetoconductance oscillations (MCO) in Sm–S junctions has been explored [17–19]. It is found that the occurrence of the MCO is due to the presence of both normal and ARs at the interface, leading to interference between the wave functions of QPs. It is this interference that results in the MCO. The interplay between the classical cyclotron motion of a QP and the phase shift caused by the magnetic field is the source of the MCO. The effects of disorder near the junction and roughness of the interface of Sm-S junctions also have been investigated [17–19]. The MCO are substantially suppressed by these effects.

In this paper, we investigate the transport properties of QPs in a modified Sm-S junction, which is composed of a superconductor (S) and a semiconductor (Sm) containing a laterally potential barrier layer inside the semiconductor region. Therefore, it forms a dual–channel quantum waveguide (DQW) of semiconductor coupled to each other by this thin isolating barrier layer. To model the imperfectness of the interface of the Sm-S junction and the magnetic penetration depth effect at the interface, we

[a] e-mail: guby@aphy.iphy.ac.cn

introduce a $\delta-$function scattering potential barrier lying close to the interface of junctions. In a previous paper [20], we have studied in detail the MCO in this pure DQW with an infinite length in the normal state. We found that the quantized conductance of such a structure as a function of Fermi energy or magnetic field exhibits square–wave–like oscillations. This feature of the conductance is closely related to the oscillatory energy-dispersion spectrum of electron. Motivated by the previous work [20], we are interested in what are the effects of this oscillatory dispersion on the properties of the MCO in the Sm-S junctions. From quantum mechanics calculations, we find that the MCO of the proposed Sm-S junctions originate from two sources: One is from interference of the wave functions of QP, due to the coexistence of both the normal and multiple ARs at the interface. The other is from the oscillatory variation of the number of propagating modes with magnetic fields. The pattern of the MCO strongly depends on the coupling strength between the two subwaveguides inside the DQW. We study the influences of various structural and physical parameters of the junctions as well as the interface scattering on the MCO in detail. To explain the MCO, we present semiclassical phenomenology calculations, similar to the paper of Asano [18], to fit the numerical results. The theoretically fitted results are in good agreement with the numerical ones.

The rest of this paper is organized as follows. In Section 2, we give a brief description of the model Sm-S junction and the necessary formulae used in the calculations. The numerical calculation results are presented in Section 3 with analyses. Finally, the conclusion is made in Section 4. In the Appendix, we present a detailed derivation, based on the BTK theory [5], of the reflective and transmissive coefficients for the electron-like and hole-like quasi-particles at the Sm-S junction under zero magnetic field and the transmissive and reflective coefficients of quasi-particle through a single barrier layer when the particle impacts obliquely upon the surface of the barrier.

2 Model Sm-S junction and calculation method

The system consists of a dual-channel quantum waveguide (DQW) in a two-dimensional electron gas (2DEG) connected to a semi-infinite superconductor (S) of width W, as shown in Figure 1. The formed Sm-S junction is aligned in the xy plane; and the DQW is located in $x \leq 0$ region, while the superconductor (type I or II) occupies the region $x > 0$. A modified Sm-S junction is produced with an interface at $x_0 = 0$. One very thin scattering barrier layer with a $\delta-$function potential of strength H is placed at the interface to simulate the imperfectness of interface and the magnetic penetration depth effect at the Sm-S interface. Two parallel quantum waveguides (QWs) are coupled through a thin layer of potential barrier with square profile of height V_0 and width ΔW. The widths of two subwaveguides are $W_{\rm I}$ and $W_{\rm II}$, respectively. Therefore, total width of the QW is $W = W_{\rm I} + W_{\rm II} + \Delta W$. The DQW is subjected to magnetic field B along the $z-$direction. In the present work, we limit the applied magnetic field only in the semiconductor region. The current flows along the $x-$direction. For simplicity, we employ a hard-wall confinement potential for the lateral boundaries of the junction. Inside the QW, the potential is set at zero.

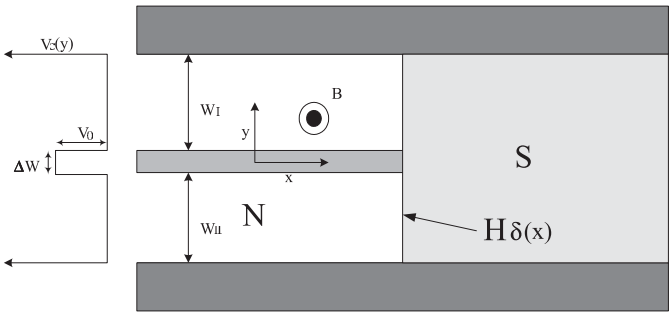

Fig. 1. Schematic view of a semiconductor-superconductor junction with a lateral potential barrier isolator inside the semiconductor region. The hatched region represents the superconductor. The dual quantum waveguides have widths of $W_{\rm I}$ and $W_{\rm II}$, they are coupled with each other through a square potential barrier with a thickness of ΔW and a height of V_0. The magnetic field B is applied in the $\widehat{z}$ direction in the semiconductor only. The $\delta-$function potential barrier is placed at the Sm-S interface to model the interface scattering effect. The inset shows the profile of the potential in the semiconductor region.

The Bogoliubov-de Gennes (BdeG) equation

$$\begin{pmatrix} H_0(\mathbf{r}) & \Delta(\mathbf{r}) \\ \Delta^*(\mathbf{r}) & -H_0^*(\mathbf{r}) \end{pmatrix} \begin{pmatrix} u(\mathbf{r}) \\ v(\mathbf{r}) \end{pmatrix} = E \begin{pmatrix} u(\mathbf{r}) \\ v(\mathbf{r}) \end{pmatrix} \qquad (1)$$

provides a microscopic formalism for studying inhomogeneous superconductors and NS interfaces [9,21]. Here, $\Delta(\mathbf{r})$ is the pairing potential and $H_0(\mathbf{r})$ represents a single-particle Hamiltonian in the effective mass approximation. We follow BTK theory [5] and neglect the effect of a finite bias on the scattering probabilities [22]. In the BdeG equation, we omit the phase of the pairing potential since only the absolute value is important for the considered geometry, and we choose the pairing potential to be uniform, Δ_0 in the superconductor and zero in the semiconductor waveguides. We also assume that the effective masses of electrons in the two materials can be different, m_N^* in semiconductor and $m_s = m_0$ in superconductor.

We employ the Landau gauge of potential vector of the magnetic field as

$$\boldsymbol{A} = \begin{cases} (0, Bx) = (-By, 0) + \boldsymbol{\nabla}(Bxy) & for \;\; x < 0, \\ (0, 0), & for \;\; x \geq 0. \end{cases} \qquad (2)$$

The single-particle Hamiltonian is given by

$$H_0 = \left[\frac{1}{2m_N^*} (\boldsymbol{P} - \frac{e}{c}\boldsymbol{A})^2 + V_c(y) + \mathrm{H}\delta(x) - \mu_N \right], \qquad (3)$$

where the transverse confining potential $V_c(y)$ is given by

$$V_c(y) = \begin{cases} \infty, & \text{when } \; |y| \geq W/2; \\ V_0, \text{ when } & -\Delta W/2 < y < \Delta W/2; \\ 0, & \text{otherwise.} \end{cases} \qquad (4)$$

μ_N indicates the Fermi energy in 2DEG. To model the scattering effect due to the imperfectness of interface and the magnetic penetration depth effect, we simply introduce a thin potential barrier with a $\delta-$function potential of strength H at interface $x_0 = 0$. After performing the gauge transformation, the solution $\tilde{\Psi}$ to equation $H_0\tilde{\Psi} = E\tilde{\Psi}$ can be expressed in a variable separation form

$$\tilde{\Psi}(x,y) = \mathrm{e}^{ikx}\tilde{\Phi}_k^E(y)\mathrm{e}^{i\frac{eB}{\hbar c}xy}, \tag{5}$$

where $\widetilde{\Phi}_k^E(y)$ satisfies the one-dimensional Schrödinger equation

$$\left\{\frac{\hbar^2}{2m_N^*}\left[(k+\frac{eB}{\hbar c}y)^2 - \frac{\partial^2}{\partial y^2}\right] + V_c(y) - \mu_N\right\}\tilde{\Phi}_k^E(y) = E\tilde{\Phi}_k^E(y). \tag{6}$$

We expand the wave function $\widetilde{\Phi}_k^E(y)$ in terms of basis $\left\{f_l(y) = \sqrt{\frac{2}{W}}\sin\left[\frac{\pi l}{W}\left(y+\frac{W}{2}\right)\right]\right\}$ as

$$\tilde{\Phi}_k^E(y) = \sum_l c_l^k f_l(y) \tag{7}$$

and use the extended basis technique [23,24], for a given positive energy E (for an electron-like QP), a set of eigenfunctions $\left\{\Phi_l^{(\pm)e}(y)\right\}$ and eigenvalues $\left\{k_l^{(\pm)e}\right\}$ can be obtained, while for a given negative energy $-E$ (for hole-like QP) again, the set $\left\{\Phi_l^{(\pm)h}(y)\right\}$ and $\left\{k_l^{(\pm)h}\right\}$ can be obtained, too. Thus, in the DQW region, when an electron-like QP at mode n is injected into the Sm-S junction, the wave function can be expressed as

$$\begin{aligned}\Psi_n^{Sm}(x,y) = &\begin{pmatrix}1\\0\end{pmatrix}\mathrm{e}^{ik_n^{(+)e}x}\Phi_n^{(+)e}(y)\mathrm{e}^{i\frac{eB}{\hbar c}xy}\\ &+\sum_l A_{ln}\begin{pmatrix}1\\0\end{pmatrix}\mathrm{e}^{ik_l^{(-)e}x}\Phi_l^{(-)e}(y)\mathrm{e}^{i\frac{eB}{\hbar c}xy}\\ &+\sum_l B_{ln}\begin{pmatrix}0\\1\end{pmatrix}\mathrm{e}^{ik_l^{(-)h}x}\Phi_l^{(-)h}(y)\mathrm{e}^{-i\frac{eB}{\hbar c}xy}.\end{aligned} \tag{8}$$

In the superconductor, the wave function can be expressed as

$$\Psi_n^S(x,y) = \sum_l C_{ln}\begin{pmatrix}\alpha_+\\ \beta_+\end{pmatrix}\mathrm{e}^{iq_l^+x}f_l(y) + \sum_l D_{ln}\begin{pmatrix}\alpha_-\\ \beta_-\end{pmatrix}\mathrm{e}^{-iq_l^-x}f_l(y), \tag{9}$$

where the wave number is given by

$$q_l^{\pm} = \sqrt{\frac{2m_0}{\hbar^2}\mu_S - \left(\frac{l\pi}{W}\right)^2 \pm i\frac{2m_0}{\hbar^2}\sqrt{|\Delta_0|^2 - E^2}}, \tag{10}$$

where μ_S denotes the Fermi energy in the superconductor. When $E < \Delta_0$, the single-particle excitations will decay in the superconductor. In this case, we have

$$\alpha_+ = \alpha_- = 1/\sqrt{2}, \tag{11a}$$

$$\beta_+ = \beta_-^* = \frac{E - i\sqrt{|\Delta_0|^2 - E^2}}{\sqrt{2}\Delta_0}. \tag{11b}$$

When $E > \Delta_0$, the relevant single-particle excitations can propagate through the superconductor. The corresponding wave function can be expressed in the well-known form $\alpha_+ = \beta_- = u_0$ and $\alpha_- = \beta_+ = v_0$ with

$$u_0^2 = \frac{1}{2}\left(1 + \frac{\sqrt{E^2 - |\Delta_0|^2}}{E}\right) = 1 - v_0^2. \tag{12}$$

By using the conventional matching technique, *i.e.*, the continuity of the wave function and its normal derivative with the inverse effective mass weight factor, the coefficients A_{ln}, B_{ln}, C_{ln}, and D_{ln} can be fully determined. According to the law of the current conservation, the current flowing through the system can be calculated in the normal region [5]

$$\begin{aligned}I(V) = \frac{2e^2}{h}\sum_{l,n}{}' \int_{-\infty}^{+\infty}&[f_0(\mu_N + E - eV) - f_0(\mu_N + E)]\\ &\times[1 - R_{ee,ln} + R_{he,ln}]dE,\end{aligned} \tag{13}$$

where f_0 denotes the Fermi distribution function and the summation $\sum_l' = N_c$ runs over the all propagating channels. The reflection probabilities for electron-like and hole-like QPs are evaluated by

$$R_{ee,ln} = \left(v_l^{(-)e}/v_n^{(+)e}\right)|A_{ln}|^2, \tag{14a}$$

$$R_{he,ln} = \left(v_l^{(-)h}/v_n^{(+)e}\right)|B_{ln}|^2, \tag{14b}$$

where $v_l^{(\pm)e,h}$ is the group velocity of the QP in channel l and given by

$$v_l^{(\pm)e} = \frac{\hbar}{m_N^*}\int_{-0.5W}^{0.5W}\Phi_l^{*(\pm)e}(y)\left[k_l^{(\pm)e} - \frac{eB}{\hbar c}y\right]\Phi_l^{(\pm)e}(y)dy, \tag{15a}$$

$$v_l^{(\pm)h} = \frac{\hbar}{m_N^*}\int_{-0.5W}^{0.5W}\Phi_l^{*(\pm)h}(y)\left[k_l^{(\pm)h} + \frac{eB}{\hbar c}y\right]\Phi_l^{(\pm)h}(y)dy. \tag{15b}$$

Using $R_{ee,ln}$ and $R_{he,ln}$ evaluated at $E = eV$, the differential conductance at $T = 0$ K and zero bias can be evaluated by the Takane-Ebisawa formula [7]

$$G(V) = \frac{\partial I}{\partial V} = \frac{2e^2}{h}\sum_{l.n}{}'\left(\delta_{l,n} - R_{ee,ln} + R_{he,ln}\right), \tag{16}$$

where l and n are the propagation channels in 2DEG under magnetic field, $R_{ee,ln}$ and $R_{he,ln}$ are evaluated at $\mu_N + E$. The current conservation law requires

$$\sum_l{}'(R_{ee,ln} + R_{he,ln}) = 1. \tag{17}$$

3 Numerical results and analyses

We now present the numerical results of magnetoconductance of QPs in the system as a function of $\beta \equiv \mu_N/\hbar\omega_c$,

where $\omega_c = eB/cm_N^*$ is the cyclotron frequency, for different parameters. β coincides with the filling factor of quantum-Hall physics when the normal region is a 2DEG. As the pair potential in superconductors is typically 1 meV and the Fermi energy in 2DEG is about 100 meV, we thus fixed $\Delta_0/\mu_N = 0.02$ throughout this paper. We also fixed the width of the wire to be $Wk_F = 40$, and the incident energy of the QPs $E/\Delta_0 = 0$.

To give a better comparison and reveal the origin of the MCO, we first display the variation of the magnetoconductance with β in two cases of the QW with and without the laterally isolating barrier layer in Figure 2a. Solid and dot-dashed curves correspond to the QW with and without isolating barrier layer, respectively. The isolating barrier layer is placed along the horizontal central line of the QW, and we set $\Delta_0 = 0.0$. In this situation, the system corresponds to a SQW (without the isolating barrier layer) Sm-N junction or a DQW (with an isolating barrier layer) Sm-N junction with an interface at which the magnetic field changes abruptly, *i.e.*, the magnetic field is a finite B for $x \leq 0$, and 0 for $x > 0$. The height of the isolating barrier is $V_0/\mu_N = 0.5$, its width $\Delta W/W = 0.05$ or 0, $m_N^*/m_0 = 1.0$, $\mu_S/\mu_N = 1.0$, $V_{bh} = k_F H/\mu_N = 0$, $k_F W = 40$, and $\mu_N = \hbar^2 k_F^2/2m_N^*$. It is clearly seen that the magnetoconductance curve (dot-dashed line) for the SQW Sm-N junction exhibits a well-known step increase with the increase of β. When increasing β, *i.e.*, when decreasing the magnetic fields, the number of the magnetic populated levels is correspondingly increased, thus, new a propagation channel is opened step-by-step, correspondingly, the next new conductance step appears. However, the leading edge of the conductance plateau, near the threshold magnetic field of new channel opening, is always rounded due to the presence of the magnetic interface at $x = 0$. It is the existence of the magnetic interface that causes the enhancement of normal electron reflection, which contributes to a negative conductance. Near every threshold magnetic field, the corresponding longitudinal (along the $x-$axis) kinetic energy of electron-like QP is much smaller than the magnetic scattering potential, therefore, the electron reflection becomes striking. However, when further decreasing the magnetic field, the longitudinal kinetic energy of the electron-like QP becomes larger than the magnetic scattering potential, thus, the electron reflection effect becomes weak and negligible and the conductance curve develops into an ideal plateau. The conductance curve (solid curve) for the DQW Sm-N junction exhibits a series of peaks superimposed upon every conductance plateau at its leading edge with the increase of β. This behavior is robust with respect to the increase or decrease of the number of the propagation channels with decreasing magnetic field. This oscillatory conductance can be well explored as coming from the dispersion behavior of electrons in the infinite long DQW, as discussed in reference [20].

We now display the variation of magnetoconductance G, in units of $2e^2/h$, with $\beta \equiv \mu_N/\hbar\omega_c$ for the SQW Sm-S junction and DQW Sm-S junction in Figures 2b and 2c, respectively. The relevant parameters are

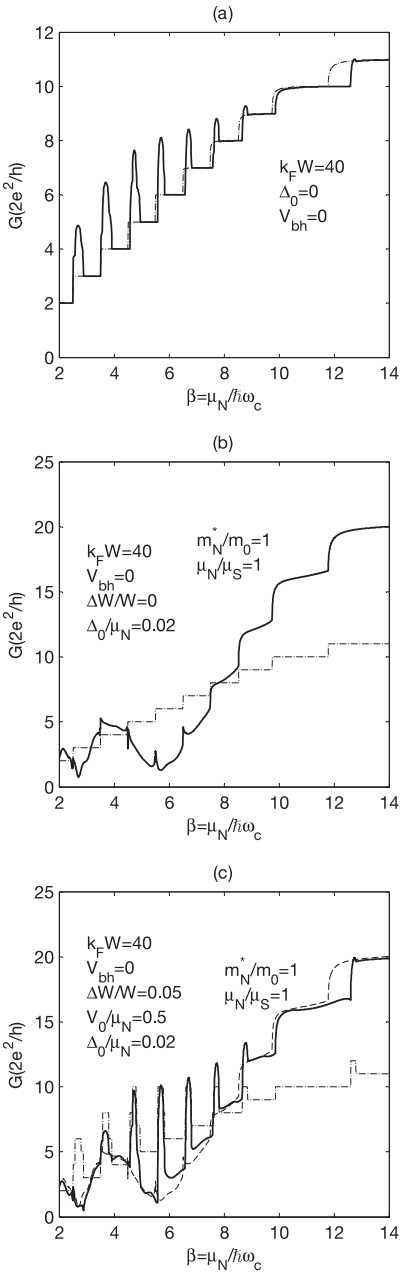

Fig. 2. (a) Calculated magnetoconductance as a function of $\beta = \mu_N/\hbar\omega_c$ for two normal state structures: One is the single QW (SQW) Sm-N junction with an interface (at $x = 0$) at which the abrupt change of magnetic fields appears, *i.e.*, the magnetic field $B = 0$ for $x \geq 0$ and B for $x < 0$; the second structure is the DQW Sm-N junction. The DQW consists of the coupled dual-channel quantum waveguides. The magnetic field only applies to the DQW region. The relevant parameters are: $V_0/\mu_N = 0.5$, $\Delta W/W = 0.05$, $\mu_S/\mu_N = 1$, $m_N^*/m_0 = 1$, $k_F W = 40$, and $V_{bh} = 0$. The solid curve corresponds to the DQW Sm-N junction and the dashed curve to the SQW Sm-N junction. (b) Calculated magnetoconductor as a function of β for the SQW Sm-S junction. The parameters are: $\Delta_0 = 0.02$, $k_F W = 40$, $m_N^*/m_0 = 1$, $\mu_N/\mu_S = 1$, and $V_{bh} = 0$. The solid curve corresponds to G in units of $2e^2/h$ and the dotted-dashed curve indicates the number N_c of the propagating channels in the SQW. (c) As Figure 2b except for DQW with $\Delta W/W = 0.05$ and $V_0/\mu_N = 0.5$.

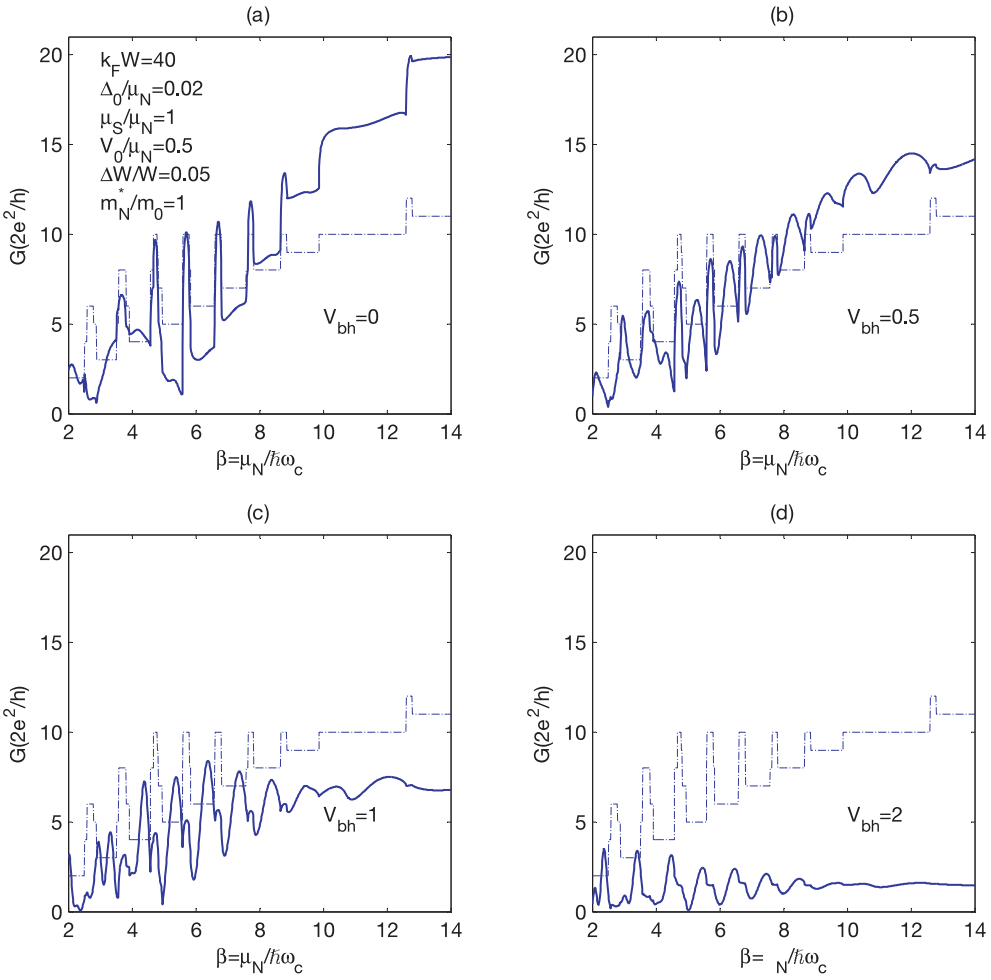

Fig. 3. Effects of the interface scattering potential on G-β plot in the DQW Sm-S junction: (a) $V_{bh} = 0.0$, (b) 0.5, (c) 1.0, and (d) 2.0, respectively. The other parameters are the same as those in Figure 2c. Solid curves correspond to G and dot-dashed curves to N_c variation for reference.

the same as those in Figure 1a, except for $\Delta_0/\mu_N = 0.02$ now. All the solid curves correspond to conductance and dot-dashed lines to the number N_c of the propagating channels in the 2DEG. Hereafter, we plot all figures in this manner. For a clear comparison, we also show the conductance curve of the SQW Sm-S junction in Figure 2c by the dashed line. In this case the AR is switched on due to the finite pair potential of the superconductor. Figure 2b is essentially the same as that of Figure 1a in reference [18]. The conductance decreases in a step manner with increase of magnetic field ($14 > \beta > 9$) in Figure 2b as the subbands are magnetically depopulated. The other hand, the Andreev reflection is active now, thus, the quantization of the conductance now is in a unit of $4e^2/h$, doubling the quantization value ($2e^2/h$) of conductance in the SQW Sm-N junction. Normal electron reflection at the interface of the abrupt change of magnetic field is the source of the appearance of the rounded corner in all the conductance plateaus.

However, in the intermediate-field region ($8 > \beta > 4.5$), G drops below the N_c-curve because the electron reflection now is significantly enhanced and the AR becomes imperfect. In the uniform SQW with $\mu_S = \mu_N$ and $m_N^* = m_0$, $R_{ee} \to 1$, consequently, only the hole-like QPs are excited from the AR and they move in skipping orbits along the interface and boundary wall. The hole-like QPs now become the major current carriers. The quantum interference of the electron wave functions disappears. The variation of magnetoconductance with magnetic fields in the DQW Sm-S junction is very different from that of the SQW Sm-S junction, as shown in Figure 2c. The profiles of G seems to be similar to the curve of Figure 2b with the exception of superimposing upon a series of peaks when $9 > \beta > 2$, which are generated from the oscillations of N_c. The position of the peaks is perfectly aligned with that of the peaks of N_c. It concludes that the whole behavior of G is essentially dominated by the variation of N_c. These oscillatory peaks are no longer caused by the quantum interference of wave functions of QPs undergoing multiple AR at the interface alone. A new mechanism of the MCO in the DQW Sm-S junction takes over now.

We now survey the effects of the scattering potential at the interface on G. The results are displayed in Figure 3 for different scattering strengths of V_{bh}: (a) $V_{bh} = 0.0$, (b) 0.5, (c) 1.0, and (d) 2.0, respectively. The other parameters remain unchanged as the same as those in

Figure 2c. It is clearly seen that when switching on the scattering potential, the profile of G is substantially modified. The effects are two-folds: (i) G exhibits striking oscillations which no longer exactly follow the oscillations of N_c. The number of oscillation peaks is more than that of N_c, (see Figs. 3b–3d). As the normal reflection of electron-like QPs at the interface now is considerably enhanced due to the introduction of scattering potential, the superposition of the multiple ARs with different phases causes the phenomenon of "beat frequency" of wave functions, which leads to large oscillations; (ii) the magnitude of G is significantly reduced from twice the value of N_c to that smaller than N_c with the increase of V_{bh}, due to the enhancement of R_{ee}.

Figure 4 displays the theoretically fitted results of the MCO in both the SQW and DQW Sm-S junctions based on a phenomenological argument (see next paragraph in detail): (a) $\mu_S/\mu_N = 1$, $m_N^*/m_0 = 1$, $V_{bh} = 0.5$, and $\Delta W/W = 0$; (b) as (a) except for $\Delta W/W = 0.05$. The other parameters are: $k_F W = 40$, $\Delta_0/\mu_N = 0.02$, and $V_0/\mu_N = 0.5$. Solid lines correspond to the numerical calculated results, dashed lines to theoretically fitted results and the dot-dashed lines refer to the N_c variation for reference. The horizontal straight line with two ended arrows in these plots indicates the magnetic field range of MCO by theoretically fitting, which satisfies the condition:

$$W/2 < L_c < W, \tag{18}$$

i.e., $10 > \beta > 5$, where $L_c \equiv 4\beta/k_F$ is the diameter of the cyclotron orbit of QPs.

To better understand the origin of the MCO in the DQW Sm-S junction, we basically follow the discussions in reference [18] to perform the relevant quantum mechanical calculations. As indicated by reference [18], by using the S-matrix in the one-dimensional Sm-S junction, we can explain the MCO behavior in the two-dimensional Sm-S junction. The cyclotron orbit of a QP plays an important role in the MCO. Figure 5 shows the schematic picture of the typical trajectories of the QP reflected at the interface of the DQW Sm-S junction. The solid and dashed lines denote the trajectory orbit of a QP in the electron and hole branches, respectively. Figure 5a shows that an electron-like QP is incident from the lower-left corner and undergoes double ARs at y_1 and y_2 at the interface. Electron like QP and the induced hole-like QP are tunneled or reflected once in the isolating barrier layer. Hereafter we refer it to as Orbit #1. The position of the orbital starting point is located at $L_c - W > y > 0$. Figure 5b shows the second class of orbits (referred to as Orbit #2), the position of this orbital starting point is located at $W/2 > y > L_c - W$. Figure 5c shows the third class of orbits (referred to as Orbit #3), The position of the orbital starting point is located at $W > y > W/2$.

We now discuss the wave functions of these three kinds of orbits of QP in detail. For Orbit #1, an incident QP is reflected doubly at the Sm-S interface, therefore, it produces four trajectories, *i.e.*, two electron branches and two hole branches, as seen in Figure 5a. The first reflected electron-like (hole-like) QP at y_1 crosses the isolating barrier layer and then undergoes the second AR at y_2 on the

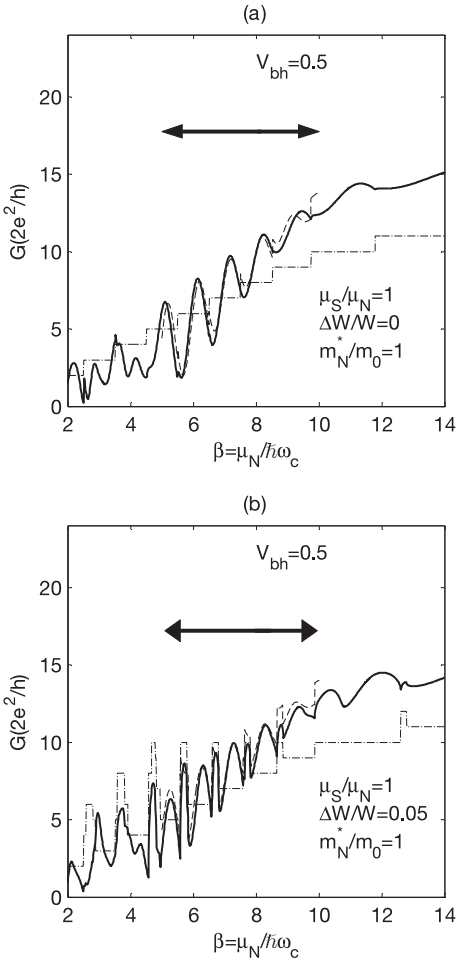

Fig. 4. Theoretically fitted results of G-β behavior in SQW Sm-S and DQW Sm-S junctions. (a) $\mu_S/\mu_N = 1.0$, $m_N^*/m_0 = 1.0$, $V_{bh} = 0.5$, $\Delta W/W = 0$ (SQW); and (b) as (a) except for $\Delta W/W = 0.05$ (DQW). The other parameters are: $k_F W = 40$, $\Delta_0/\mu_N = 0.02$, and $V_0/\mu_N = 0.5$. The numerical results are shown by solid curves while the theoretically fitted results are shown by the dashed curves. The variation of N_c is indicated by dot-dashed lines. The horizontal straight line with two ended arrows indicates the relevant magnetic field range in which the theoretically fitted calculation is achieved.

interface, and then impacts upon the upper boundary wall of the DQW and moves along the upper wall of the QW in a skipping manner. The QP acquires two additional phases: One is from the cyclotron motion of the QP in the magnetic field, *i.e.*, travelling from y_1 to y_2 along a half circle, and the other comes from the tunneling process of the QP through the isolating barrier layer. The gained extra phase in the cyclotron motion for the electron-like QP is $\phi_B = (e/\hbar c)\int_{y_1}^{y_2} d\mathbf{r}\mathbf{A}\cdot(\mathbf{r}) = -\pi\beta$, while the gained extra phase for the hole-like QP is $-\phi_B$ [18], because the charge of the hole-like QP is opposite to that of the electron-like QP, therefore, the direction of the cyclotron motion of the hole-like QP is opposite to that of the electron-like QP. In the following, we will decompose the transport processes of the QP into several sub-trajectories. We first consider the double ARs at the Sm-S interface, once transmission

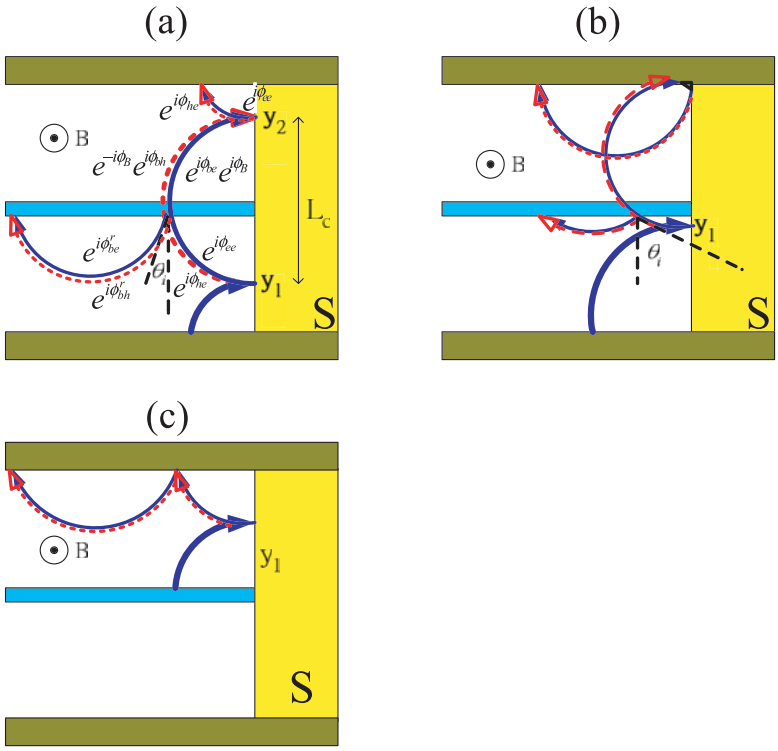

Fig. 5. Schematic picture of various trajectories of the QPs, travelling in the DQW Sm-S junction. The solid and dashed lines denote the trajectory motion of an electron-like QP and hole-like QP, respectively. $L_c \equiv 4\beta/k_F$ is the diameter of the cyclotron orbit.

and once reflection at the isolating barrier layer by using the S-matrix in the one-dimensional case. The effects of the magnetic fields (ϕ_B), the tunneling ($\phi_{be,bh}$) and the reflection ($\phi^r_{be,bh}$) in the isolating barrier layer are ascribed to an appropriate phase shift in the wave function of QP, as described below:

$$\Psi_1^{e(1)} = |r_{ee}|e^{i\phi_{ee}} \cdot |t_{be}|\mathrm{e}^{i\phi_{be}} \cdot \mathrm{e}^{i\phi_B} \cdot |r_{ee}|\mathrm{e}^{i\phi_{ee}}, \tag{19a}$$

$$\Psi_2^{e(1)} = |r_{eh}|\mathrm{e}^{i\phi_{eh}} \cdot |t_{bh}|\mathrm{e}^{i\phi_{bh}}\mathrm{e}^{-i\phi_B} \cdot |r_{he}|\mathrm{e}^{i\phi_{he}} \tag{19b}$$

$$\Psi_3^{h(1)} = |r_{he}|\mathrm{e}^{i\phi_{he}} \cdot |t_{be}|\mathrm{e}^{i\phi_{be}} \cdot \mathrm{e}^{i\phi_B} \cdot |r_{ee}|\mathrm{e}^{i\phi_{ee}}, \tag{19c}$$

$$\Psi_4^{h(1)} = |r_{hh}|\mathrm{e}^{i\phi_{hh}} \cdot |t_{bh}|\mathrm{e}^{i\phi_{bh}} \cdot \mathrm{e}^{-i\phi_B} \cdot |r_{he}|\mathrm{e}^{i\phi_{he}}, \tag{19d}$$

$$\Psi_5^{re(1)} = |r_{be}|\mathrm{e}^{i\phi^r_{be}} \cdot |r_{ee}|\mathrm{e}^{i\phi_{ee}},$$

for electron reflection at isolator layer, (19e)

$$\Psi_6^{rh(1)} = |r_{bh}|\mathrm{e}^{i\phi^r_{bh}} \cdot |r_{he}|\mathrm{e}^{i\phi_{he}},$$

for hole reflection at isolator layer. (19f)

The two paths of the QP in the electron branch interfere with each other and $|\Psi_1^{e(1)} + \Psi_2^{e(1)}|^2$ is the reflection probability for electron-like QP, while $|\Psi_3^{h(1)} + \Psi_4^{h(1)}|^2$ is the reflection probability for hole-like QP. However, $\Psi_5^{re(1)}(\Psi_6^{rh(1)})$ does not participate in the quantum interference process because the trajectory, when approaching the isolating barrier layer, deviates from the trajectory of the QP described by $\Psi_1^{e(1)}$ and $\Psi_2^{e(1)}$, therefore, they never meet with each other. The contribution of Orbit #1 to G is evaluated as

$$G_1 = \Theta(y)\Theta((W - L_c) - y) \cdot \left(\frac{2e^2}{h}\right) \widetilde{N}_c \cdot p_1(\beta) \times \left[\left|\Psi_3^{h(1)} + \Psi_4^{h(1)}\right|^2 - \left|\Psi_1^{e(1)} + \Psi_2^{e(1)}\right|^2 + \left|\Psi_6^{rh(1)}\right|^2 - \left|\Psi_5^{re(1)}\right|^2 \right], \tag{20}$$

where $\Theta(y)$ represents a Heaviside function, *i.e.*, $\Theta(y) = 1$ when $y \geq 0$, while 0 when $y < 0$. $p_1(\beta)$ is a probability weight factor of different orbits. $\widetilde{N}_c$ denotes the effective number of the propagating modes in the DQW.

Similarly, for Orbit #2 in Figure 5b, we have

$$\Psi_1^{e(2)} = |t_{be}|\mathrm{e}^{i\phi_{be}} \cdot \mathrm{e}^{i\phi_B} \cdot |r_{ee}|\mathrm{e}^{i\phi_{ee}}, \tag{21a}$$

$$\Psi_2^{h(2)} = |t_{bh}|\mathrm{e}^{i\phi_{bh}} \cdot \mathrm{e}^{-i\phi_B} \cdot |r_{he}|\mathrm{e}^{i\phi_{he}}, \tag{21b}$$

$$\Psi_3^{re(2)} = |r_{be}|\mathrm{e}^{i\phi^r_{be}} \cdot |r_{ee}|\mathrm{e}^{i\phi_{ee}},$$

for electron reflection at isolator layer, (21c)

$$\Psi_4^{rh(2)} = |r_{bh}|\mathrm{e}^{i\phi^r_{bh}} \cdot |r_{eh}|\mathrm{e}^{i\phi_{eh}},$$

for hole reflection at isolator layer. (21d)

The contribution of Orbit #2 to G is

$$G_2 = \Theta(y-(W-L_c))\Theta(W/2-y)\cdot\left(\frac{2e^2}{h}\right)\widetilde{N}_c \times p_2(\beta)\left[\left|\Psi_2^{h(2)}\right|^2-\left|\Psi_1^{e(2)}\right|^2+\left|\Psi_4^{rh(2)}\right|^2-\left|\Psi_3^{re(2)}\right|^2\right]. \quad (22)$$

Finally, for Orbit #3, we have

$$\Psi_1^{e(3)} = |r_{ee}|\mathrm{e}^{i\phi_{ee}}(at\ y_1), \quad (23a)$$

$$\Psi_2^{h(3)} = |r_{he}|\mathrm{e}^{i\phi_{he}}(at\ y_1). \quad (23b)$$

and the contribution of Orbit #3 to G is

$$G_3 = [\delta_{N_c,\tilde{N}_c}\Theta(L_c-y)+(1-\delta_{N_c,\tilde{N}_c})\Theta(W-y)] \times\Theta(y-W/2)\cdot\left(\frac{2e^2}{h}\right)\widetilde{N}_c \times p_3(\beta)\left[\left|\Psi_2^{h(3)}\right|^2-\left|\Psi_1^{e(3)}\right|^2\right]. \quad (24)$$

The total magnetoconductance G can be calculated as

$$G = \frac{2e^2}{h}\widetilde{N}_c+\frac{1}{W}\sum_{y=0}^{y=W}[G_1+G_2+G_3]\,/ \int_0^W dy\Theta(y)\left[\delta_{N_c,\tilde{N}_c}\Theta(L_c-y)+(1-\delta_{N_c,\tilde{N}_c})\Theta(W-y)\right]. \quad (25)$$

To complete the relevant calculations, we need to exactly estimate the related coefficients, such as r_{ee}, r_{he}, r_{hh}, r_{he}, t_{be}, t_{bh}, r_{be}, and r_{bh}, (see the Appendix for details).

We consider that some circular orbits of the QP may directly cross and arrive at the upper boundary wall of the DQW without touching the Sm-S interface, we introduce an approximate weight factor for trajectory circles as $p_1(\beta) = p_2(\beta) = p_3(\beta) = 1$, and $G_2 = G_3$ when $N_c = \tilde{N}_c$. During the fitted procedure, to acquire the better fitting results, we introduce two auxiliary adjusting parameters, η_1 and η_2, such that $\left[\eta_1\left|\Psi_2^{h(3)}\right|^2-\eta_2\left|\Psi_1^{e(3)}\right|^2\right]$ with $\eta_1 = 0.8$ and $\eta_2 = 1.2$, instead of the original form of $\left[\left|\Psi_2^{h(3)}\right|^2-\left|\Psi_1^{e(3)}\right|^2\right]$ in equation (24). The necessity of these two auxiliary parameters may represent the correction for the two-dimensionality of the system.

Regarding the effective number N_c of the propagating modes, we prefer to refer to the results presented in reference [20]. It indicates that for the DQW, in the resonant-tunneling regime, a pair of edge states around the barrier layer with oppositely moving directions are coupled with each other and form a circulating localized state, leading to the quenching of the related propagating modes (formation of vortex flow). This orbit does not contribute any net current, thus, we need to subtract these orbits. We assume that the number of quenching modes is $\Delta N_c = 0.5[N_c-\nu/2]\Theta\left(N_c-\nu/2-2\right)$ from the numerical simulations, where $\nu/2 = (\beta+1/2)$ denotes the half filling factor of the Landau levels of bulk materials in magnetic fields. Finally, we have

$$\widetilde{N}_c = N_c - \Delta N_c. \quad (26)$$

We employ these equations to fit the MCO curves, the fitted results are illustrated by the dashed lines in Figures 4a and b. The horizontal straight line with two ended arrows in the plots indicates the fitting range of magnetic fields. It is evident that the theoretically fitted results are in good agreement with the numerical ones.

4 Conclusions

We present the numerical simulations to reveal the magnetoconductance oscillations (MCO) in junctions formed by a superconductor (S) and a semiconductor (Sm). In the semiconductor region, the dual-parallel coupled quantum waveguides (DQW) are coupled through a thin isolating barrier layer. We also introduce a thin barrier with the $\delta-$function potential at the Sm-S interface to model the imperfectness of the Sm-S interface and magnetic penetration depth effect. From the detailed analyses on the obtained numerical results, we conclude that the origin of the MCO in this modified Sm-S junction has two sources: One is the usual interference effect of wave functions of quasiparticles (QPs) undergoing multiple ARs at the Sm-S interface; the other stems from the oscillatory variation of the number of propagating modes when introducing the isolating barrier layer in the DQW. We propose a physical picture of the MCO within a framework of phenomenological argument to explain the MCO spectrum, and theoretically fitted results are in good agreement with numerical ones. Multiple ARs of QP at the Sm-S interface produce various trajectories of QP, and the interplay between the classical cyclotron motion of the QP and the phase shift of the QP by magnetic field and the isolating barrier layer plays an important role for the MCO. The oscillatory variation of the number N_c of the propagating modes in the DQW strongly modifies the MCO. The MCO peaks always are aligned with the peaks of N_c. It is anticipated that the MCO can be controlled by appropriately adjusting physical and structural parameters of the DQW Sm-S junctions.

One of authors (B.Y. Gu) is grateful for the hospitality of the National Science Council, Taiwan and the Electrophysics Department, National Chiao Tung University, Hsinchu, Taiwan. This work was supported by the National Science Council of the Republic of China through Grant No. NSC 90-2112-M-009-028 and the National Natural Science Foundation of China.

Appendix

To complete the relevant calculations of the MCO in the DQW Sm-S junction, we need to exactly determine the

related coefficients of r_{ee}, r_{he}, r_{hh}, r_{he}, t_{be}, t_{bh}, r_{be}, and r_{bh}. We follow BTK [5] and consider that an electron-like QP is incident inclined with an angle θ_{in} with respect to the normal direction of the interface and it impinges onto the Sm-S interface from the semiconductor at zero magnetic field. The Sm-S junction possesses different effective masses of electron, m_N^* (semiconductor region) and m_0 (S region), as well as different Fermi energies μ_N (semiconductor region) and μ_S (S region). At the interface it has an amplitude a of undergoing AR, b of electron-like QP reflection, c of electron-like QP transmission, and d of hole-like QP transmission. The scattering effect at the interface is modelled by a δ-function potential barrier $\mathrm{H}\delta(x)$ and $V_{bh} = 2m_N^*\mathrm{H}/\hbar^2 k_F$. By using the standard matching technique with the appropriate boundary conditions [5], we can derive the relevant coefficients as

$$r_{he} = a = 2(q_m + q_p)k_p u_0 v_0/\gamma, \tag{A.1a}$$

$$r_{ee} = b = \Big[u_0^2(q_m + k_m - iV_{bh})(-q_p + k_p - iV_{bh}) - v_0^2(q_m + k_p - iV_{bh})(-q_p + k_m - iV_{bh})\Big]/\gamma, \tag{A.1b}$$

$$t_{ee} = c = 2k_p u_0(q_m + k_m - iV_{bh})/\gamma, \tag{A.1c}$$

$$t_{he} = d = 2k_p v_0(q_p - k_m + iV_{bh})/\gamma, \tag{A.1d}$$

$$\gamma = u_0^2(q_m + k_m - iV_{bh})(q_p + k_p + iV_{bh}) - v_0^2(q_m - k_p - iV_{bh})(q_p - k_m + iV_{bh}), \tag{A.1e}$$

where

$$q_{p(m)} = \sqrt{\frac{m_N^*}{m_0}}\sqrt{\frac{\mu_S}{\mu_N} - \sin^2(\theta_{in}) \pm i\sqrt{(|\Delta_0|^2 - E^2)/\mu_N}}, \tag{A.2a}$$

$$k_{p(m)} = \sqrt{1 - \sin^2(\theta_{in}) \pm \frac{E}{\mu_N}}. \tag{A.2b}$$

For the incident hole-like QP from the normal side, we have an amplitude b' of undergoing AR, a' of electron reflection, c' of hole-like QP transmission, and d' of electron-like QP transmission. Also by employing the standard matching technique with the appropriate boundary conditions, we can get the relevant coefficients as

$$r_{eh} = a' = 2(q_m + q_p)k_m u_0 v_0/\gamma, \tag{A.3a}$$

$$r_{hh} = b' = \Big[u_0^2(q_p + k_p + iV_{bh})(-q_m + k_m + iV_{bh})) - v_0^2(q_p + k_m + iV_{bh})(-q_m + k_p + iV_{bh})\Big]/\gamma, \tag{A.3b}$$

$$t_{hh} = c' = 2k_m u_0(q_p + k_p + iV_{bh})/\gamma, \tag{A.3c}$$

$$t_{eh} = d' = 2k_m v_0(q_m - k_p - iV_{bh})/\gamma. \tag{A.3d}$$

u_0 and v_0 are given by equations (11a, 11b), and (12) in the text. We then easily find

$$u_0(E) = u_0(-E);\ \ v_0(E) = -v_0^*(-E);$$
$$k_p(E) = k_m(-E);\ \ q_p(\pm E) = q_m^*(\pm E).$$

Using these relations, we can obtain the general relationships

$$\gamma^*(E) = \gamma(-E);\ \ r_{ee} = r_{hh}^*(-E); r_{he}(E) = -r_{eh}^*(-E);$$
$$t_{ee}(E) = t_{hh}^*(-E);\ t_{he}(E) = -t_{eh}^*(-E). \tag{A.4}$$

In the limit of $\Delta_0 < \mu_N$ and $E = 0$, the above mentioned expressions can be reduced to [18]

$$r_{ee} = \sqrt{(1 - |\xi|^2)^2 + (2Im\xi)^2}/(1 + |\xi|^2)\mathrm{e}^{i\phi_{ee}} = r_{hh}^*, \tag{A.5a}$$

$$r_{he} = 2Re\xi/(1 + |\xi|^2)\mathrm{e}^{-i\pi/2} = r_{eh}, \tag{A.5b}$$

where

$$\xi = \sqrt{(m_N^*/\mu_0)(\mu_S/\mu_N)} + iV_{bh},$$

and

$$\tan\phi_{ee} \approx 2V_{bh}/[(m_N^*/m_0)(\mu_S/\mu_N) - 1 + V_{bh}^2].$$

Therefore, we have

$$\phi_{hh} = -\phi_{ee};\ |r_{ee}| = |r_{hh}|;$$
$$\phi_{he} = \phi_{eh} = -\pi/2; |r_{he}| = |r_{eh}|. \tag{A.6}$$

When $\xi = 1$, we have $|r_{ee}| = 0$. By using $R_{ee,ln} = 0$ and the current conservation law, the conductance is $G = (4e^2/h)N_c$, where N_c is the number of the propagation channels. In this situation, the AR becomes perfect.

We now calculate the transmissive and reflective coefficients of the electron when it is incident with an oblique angle θ_i with respect to the transverse normal of the isolating barrier layer. The barrier height is V_0 and its width is ΔW.

Through standard calculations, we can get

$$t_{be} = |t_{be}|\mathrm{e}^{i\phi_{be}}, \tag{A.7a}$$

$$|t_{be}| = \frac{1}{\sqrt{[\cosh^2(\chi k_F \Delta W) + (\frac{\chi}{2k})^2(1 - k^2/\chi^2)^2\sinh^2(\chi k_F \Delta W)]}}, \tag{A.7b}$$

$$\phi_{be} = -kk_F\Delta W + \tan^{-1}\left[-\frac{\chi}{2k}(1 - k^2/\chi^2)\tanh(\chi k_F \Delta W)\right], \tag{A.7c}$$

and

$$r_{be} = |r_{be}|\mathrm{e}^{i\phi_{be}^r}, \tag{A.8a}$$

$$|r_{be}| = \left(1 + \frac{k^2}{\chi^2}\right)\sinh(\chi k_F \Delta W) \times \frac{1}{\sqrt{[(1 - k^2/\chi^2)^2\sinh^2(\chi k_F \Delta W) + (2k/\chi)^2\cosh^2(\chi k_F \Delta W)]}}, \tag{A.8b}$$

$$\phi^r_{be} = \tan^{-1}\left[\left(\frac{2k}{\chi}\right)\frac{1}{1-k^2/\chi^2}\coth(\chi k_F \Delta W)\right], \quad \text{(A.8c)}$$

where

$$k = \sqrt{1-\sin\theta_i + E/\mu_N},$$
$$\chi = \sqrt{(V_0 - 1 - E)/\mu_N + \sin\theta_i},$$

and

$$\theta_i = [W/2 - (y + L_c/2)]/(L_c/2) = \frac{W}{L_c} - 1 - \frac{2y}{L_c}.$$

For the incident hole-like QP, we have $t_{bh}(E) = t^*_{be}(-E)$, $|t_{be}(E)| = |t_{bh}(-E)|$, $\phi_{bh}(E) = -\phi_{be}(-E)$; $r_{bh}(E) = r^*_{be}(-E)$, $|r_{be}(E)| = |r_{bh}(-E)|$, and $\phi^r_{bh}(E) = -\phi^r_{be}(-E)$; thus, we get $|t_{be}(E)|^2 + |r_{be}(E)|^2 = |t_{bh}(E)|^2 + |r_{bh}(E)|^2 = 1$.

References

1. B.J. van Wees, H. Takayanagi, in *Mesoscopic Elecron Transport,* edited by L.L. Sohn, L.P. Kouwenhoven, G. Schön, NATO ASI, Ser. E, Vol. 345 (Kluwer Academic, Dordrecht, 1997)
2. C.W.J. Beenakker, Phys. Rev. B **46**, 12841 (1992); Rev. Mod. Phys. **69**, 731 (1997); in *Mesoscopic Quantum Physics,* edited by E. Akkermans, G. Montambaux, J.-L. Pichard (North-Holland, Amsterdam, 1995)
3. A.F. Morpurgo, S. Holl, B.J. van Wees, T.M. Klapwijk, G. Borghs, Phys. Rev. Let. **78**, 2636 (1997)
4. G. Bastian, E.O. Göbel, A.B. Zorin, H. Schlze, J. Niemeyer, T. Weimann, M.R. Benett, K.E. Singer, Phys. Rev. Lett. **81**, 1686 (1998)
5. G.E. Blonder, M. Tinkham, T.M. Klapwijk, Phys. Rev. B **25**, 4515 (1982); G.E. Blonder, M. Tinkham, Phys. Rev. B **27**, 112 (1983)
6. C.J. Lambert, R. Raimondi, J. Phys. Cond. Matt. **10**, 901 (1998); C.J. Lambert, J. Phys. Cond. Matt. **3**, 6579 (1991)
7. Y. Takane, H. Ebisawa, J. Phys. Soc. Jpn **61**, 1685 (1992); *ibid.* 2858 (1992)
8. Y. Takagaki, Phys. Rev. B **57**, 4009 (1998); Y. Takagaki, H. Takayanagi, Phys. Rev. B **53**, 14530 (1996); Y. Takagaki, K. Ploog, Phys. Rev. B **51**, 7017 (1995); Superlatt. Microstruct. **25**, 659 (1999)
9. N.A. Mortensen, K. Flensberg, A.-P. Jauho, Phys. Rev. B **59**, 10176 (1999); and references therein
10. J.X. Zhu, Z.D. Wang, H.X. Tang, Phys. Rev. B **54**, 7354 (1996)
11. H. Hoppe, U. Zülicke, G. Schön, Phys. Rev. Let. **84**, 1804 (2000)
12. F. Pierre, A. Anthore, H. Pothier, C. Urbina, D. Esteve, Phys. Rev. Let. **86**, 1078 (2001)
13. A.F. Andreev, Zh. Eksp. Teor. Fiz. **46**, 1823 (1964) [Sov. Phys. JETP **19**, 1228 (1964)]; **51**, 1510 (1966) [**24**, 1019 (1967)]
14. Y. Imry, *Introduction to Mesoscopic Physics* (Oxford University Press, INC., Oxford, 1997), Chap. 7
15. H. Takayanagi, T. Akazaki, Physica B **249–251**, 462 (1998)
16. T.D. Moore, D.A. Williams, Phys. Rev. B **59**, 7308 (1999)
17. Y. Takagaki, K.H. Ploog, Phys. Rev. B **58**, 7162 (1998)
18. Y. Asano, Phys. Rev. B **61**, 1732 (2000)
19. Y. Asano, T. Yuito, Phys. Rev. B **62**, 7477 (2000)
20. J.R. Shi, B.Y. Gu, Phys. Rev. B **55**, 9941 (1997)
21. P.G. de Gennes, *Superconductivity of Metals and Alloys* (Benjamin, New York, 1999)
22. M. Kupka, Physica C **281**, 91 (1997)
23. H. Tamura, T. Ando, Phys. Rev. B **44**, 1792 (1991)
24. S. Chaudhuri, S. Bandyopadhyyay, J. Appl. Phys. **71**, 3027 (1992)